

## HiRISE observations of gas sublimation-driven activity in Mars' southern polar regions: I. Erosion of the surface

C.J. Hansen<sup>\*</sup>, N. Thomas, G. Portyankina, A. McEwen, T. Becker, S. Byrne, K. Herkenhoff, H. Kieffer, M. Mellon

Jet Propulsion Laboratory, California Institute of Technology, 4800 Oak Grove Dr., Pasadena, CA 91109-8099, United States

### ARTICLE INFO

#### Article history:

Received 4 November 2008

Revised 5 June 2009

Accepted 14 July 2009

Available online 28 July 2009

#### Keyword:

Mars, Polar caps

### ABSTRACT

The High Resolution Imaging Science Experiment (HiRISE) on the Mars Reconnaissance Orbiter (MRO) has imaged the sublimation of Mars' seasonal CO<sub>2</sub> polar cap with unprecedented detail for one complete martian southern spring. In some areas of the surface, beneath the conformal coating of seasonal ice, radially-organized channels are connected in spidery patterns. The process of formation of this terrain, erosion by gas from subliming seasonal ice, has no earthly analog. The new capabilities (high resolution, color, and stereo images) of HiRISE enable detailed study of this enigmatic terrain. Two sites are analyzed in detail, one within an area expected to have translucent seasonal CO<sub>2</sub> ice, and the other site outside that region. Stereo anaglyphs show that some channels grow larger as they go uphill – implicating gas rather than liquid as the erosive agent. Dark fans of material from the substrate are observed draped over the seasonal ice, and this material collects in thin to thick layers in the channels, possibly choking off gas flow in subsequent years, resulting in inactive crisscrossing shallow channels. In some areas there are very dense networks of channels with similar width and depth, and fewer fans emerging later in the season are observed. Subtle variations in topography affect the channel morphology. A new terminology is proposed for the wide variety of erosional features observed.

© 2009 Elsevier Inc. All rights reserved.

### 1. Introduction

Every southern winter a seasonal carbon dioxide cap covers the south pole of Mars, reaching from the pole to ~50S. In the spring-time the basal sublimation of this seasonal ice layer actively erodes the surface, forming enigmatic surface terrain morphologies with no earthly analogs. In some areas (documented by Piqueux et al. (2003)), radially-organized channels in the substrate that narrow down to thin troughs are connected in branching patterns. Every spring dark fan-shaped deposits are observed on top of the seasonal ice, which then slowly blend into the darkening background as the season progresses. This is the first of three papers that describe surface morphology and sublimation-driven activity in specific areas of Mars' south polar region as observed by the High Resolution Imaging Science Experiment (HiRISE) onboard NASA's Mars Reconnaissance Orbiter (MRO) spacecraft. HiRISE has taken over 200 very high-resolution images (~0.25 m/pixel spatial scale, thus sub-meter resolution) to study sublimation of Mars' CO<sub>2</sub> ice cap at a limited number of sites, listed in Table 1, throughout southern spring. HiRISE's high signal to noise ratio (SNR) facilitates imaging at low light levels, which allows imaging of the sublimation process to start just after the Sun rises at latitudes equivalent

to Mars' Antarctic circle. The capability of the MRO spacecraft to roll off-nadir and image features at different emission angles enables the acquisition of stereo pairs and production of anaglyphs. Near the pole, MRO's orbit groundtracks are closely spaced, enabling image acquisition at a given location with just one orbit (~112 min) separation. Here in Paper I, we describe the erosional features that result from basal sublimation and venting of the seasonal cap, which produces a confined flow of compressed gas and fines, ultimately eroding the surface, seen with unprecedented resolution in HiRISE images. We explore their relationship to local terrain, and propose a new nomenclature. Paper II (Thomas et al., this issue) describes the sublimation process, gas venting, and the deposits that appear seasonally due to inferred gas jet activity. Paper III (Portyankina et al., this issue) models the physics of key aspects of the cleaning of the translucent ice, rupture of the ice, and the release of gas.

In Section 1 of this paper we review previous studies of the sublimation process in the south polar region of Mars and the HiRISE observational campaign. This also serves as background for Papers II and III. We describe an example of this alien gas-eroded terrain and introduce new terminology.

In Section 2, we focus on two specific case studies – “Manhattan” and “Inca City”, informal names for the locations shown in Fig. 1. Manhattan is a region within the cryptic terrain (a large region near the south pole of Mars termed “cryptic” because even

<sup>\*</sup> Corresponding author.

E-mail address: [Candice.j.Hansen@jpl.nasa.gov](mailto:Candice.j.Hansen@jpl.nasa.gov) (C.J. Hansen).

**Table 1**  
Seasonal targets acquired by HiRISE. The number of sites that can be imaged by HiRISE in a single spring season is limited by data volume. A single 6 km × 12 km image can be ~0.5 GB. Instead of going after broad spatial coverage we have emphasized temporal coverage, in order to study the sublimation process as it evolves through the spring. The sites listed below have at least three images taken at different times.

Latitude (°)	Longitude East (°)	Number of observations	$L_s$ range (°)	Comment/informal name
–74.1	168.6	8	161–212	Caterpillar
–77.6	132.0	4	175–217	Cryptic terrain
–81.3	295.7	9	174–343	Inca City
–84.25	242.0	10	182–297	Starfish
–84.55	118.5	6	194–244	Finger Lake 1
–84.6	118.5	4	182–255	Finger Lake 2
–84.3 to –84.9	65.7	16	184–305	Giza
–85.0	95.0	10	195–336	Manhattan
–85.2	181.4	21	185–294	Ithaca
–85.4	103.9	14	191–293	Manhattan
–85.4	83.4	9	189–335	Oswego
–86.25	99.0	7	215–295	Manhattan
–86.4	99.0	10	181–325	Manhattan
–86.5	157.9	6	183–330	Early summer lag
–86.95	99.98	4	207–242	Manhattan – all lace
–86.99	98.7	7	186–304	Manhattan
–87.0	86.4	3	205–237	Oswego edge
<i>Dunes</i>				
–54.2	12.9	11	136–323	Russell Crater dunes
–72.0	179.4	23	160–340	Richardson dunes

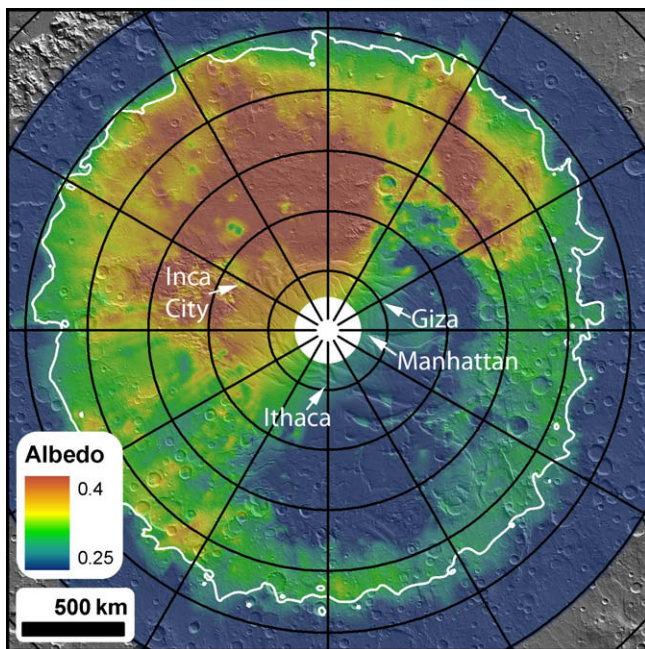


**Fig. 1.** Mars Odyssey Thermal Emission Spectrometer (TES) albedo data draped over a MOLA shaded relief background shows considerable brightness variations within the seasonal cap during the seasonal range of  $L_s$  220–225°. The white contour demarks the edge of the seasonal  $\text{CO}_2$  cap as determined from simultaneously acquired thermal data. The low albedo region from 2 o'clock (300W) to 7 o'clock (160W), within the thermally defined extent of the seasonal cap (at lower right), is the cryptic region. These data are taken from the first extended mission of Mars Global Surveyor. Meridians and parallels are spaced every 30° and 5°, respectively. The zero meridian is pointing straight up. The indicated regions (with informal names) are areas that were selected for repeated coverage throughout the spring. Manhattan in particular was selected based on earlier observations from Odyssey's THEMIS instrument (Christensen et al., 2005).

though its albedo darkens in the spring it retains the 145 K temperature of  $\text{CO}_2$  ice until late in the season) which contains a host of phenomena that are inferred to arise from local gas jet activity (Kieffer, 2000; Christensen et al., 2005; Kieffer et al., 2006). Inca City is outside the cryptic region however it also shows evidence

of gas jet activity in the form of fan-shaped deposits and morphology of the eroded surface. We compare and contrast the erosional morphologies within the cryptic terrain where the translucent ice postulate is important, and outside the cryptic region, where this model has not previously been applied because evidence for translucent  $\text{CO}_2$  ice has not been observed.

In Section 3 we propose a new nomenclature for what has been described in the past as a “zoo” (Kieffer, 2007). Past papers have applied the colloquial term “spider” to describe surface features with radially-organized channels inferred to have been carved by gas flow (Malin and Edgett, 2001; Piqueux et al., 2003). In this paper we advocate use of the term “araneiform” (spider-like) to avoid confusion with forms of Earth life, however, we may still refer to a single feature as a spider. The diversity of morphologies leads to our proposal for a new terminology for the numerous erosional features imaged by HiRISE.

It is apparent from HiRISE observations that, even within a single 6 × 12 km HiRISE image, there is also considerable variety of surface expression of these processes, which we discuss in Section 4. The influence of topography as one of the drivers is explored. We end with Section 5 that summarizes findings and future observational objectives and campaigns.

### 1.1. Scientific background

The principle of the seasonal expansion and contraction of the polar caps of Mars as a consequence of  $\text{CO}_2$  sublimation and condensation was first described by Leighton and Murray (1966) and its effect on the atmospheric pressure of Mars has been quantified on numerous occasions (e.g. Hess et al., 1979). The mass budget of the seasonal cap estimated from energy balance ranges from 800 to 1200 kg/m<sup>2</sup> (Kieffer and Titus, 2001), consistent with neutron measurements from the Mars Odyssey High Energy Neutron Detector (Litvak et al., 2007). Mars Orbiter Laser Altimeter (MOLA) and Gamma Ray Spectrometer (GRS) data have been used to establish that the depth of accumulated  $\text{CO}_2$  ice in winter is a function of latitude, typically of the order of 0.5–1 m, depending on what is assumed for the density (Smith et al., 2001; Aharonson et al., 2004; Kelly et al., 2006; Litvak et al., 2007).

While sublimation in spring and summer was expected to be affected by ice albedo and topographic effects (Leighton and Murray,

1966), it was not until high resolution data from the Mars Orbiter Camera showed the presence of dynamic features on the surface, such as fan-shaped dark patches, that rather more exotic processes were also thought to be at work (Malin and Edgett, 2001). The fans have been interpreted as due to a mechanism with similarity to that suggested for the plumes of Triton (Smith et al., 1989; Soderblom et al., 1990; Kirk et al., 1990). On Mars it is the optical properties of CO<sub>2</sub> slab ice, which can be translucent at visible wavelengths but opaque in the thermal infrared, depending on grain size (Hansen, 1997, 2005) that are key to fan formation: Kieffer (2000) suggested that, in spring, sunlight would pass through a translucent impermeable CO<sub>2</sub> ice slab and heat the optically opaque ground below. CO<sub>2</sub> sublimation is then initiated from the bottom of the ice layer. The gas is trapped under pressure, released either explosively or continuously through weak spots in the otherwise impermeable ice layer, entraining loose fine material from the ground below the ice slab, and then lofting the fines up above the top of the seasonal ice to be carried downwind and deposited (Kieffer et al., 2006).

One challenge to the translucent ice/gas jet hypothesis was raised by Aharonson (2004). He pointed out that spots and fans were visible in MOC images in polar twilight, and advocated conduction of thermal energy stored in the ground during summer months as an additional source of sublimation energy to the bottom of the ice slab in the spring before sunrise.

Piqueux et al. (2003) tested the hypothesis that radially-organized troughs (“spiders”) observed in the southern polar region were a result of the gas-venting process, with the “spiders” channeling sublimating gas to the gas vents, entraining loose surface material. They mapped the distribution of araneiform structures over the south polar region and noted that they were concentrated in the cryptic region, consistent with Kieffer’s translucent ice postulate.

Erosion of channels is proposed to occur by entrainment of loose desiccated surface material once the flow velocity exceeds the saltation threshold (Kieffer, 2007). Below the seasonal CO<sub>2</sub> ice at high southern latitudes the ground should have a layer of poorly consolidated soil, then a cemented mixture of water ice and soil (Boynton et al., 2003; Titus et al., 2003). The water ice level at these latitudes is ~5–10 cm below the surface of the ground (Mellon and Phillips, 2001; Mellon et al., 2004; Prettyman et al., 2004). Closer to the surface (and away from the edge of the perennial cap), the water will diffuse out to the atmosphere, leaving behind desiccated soil (Schorghofer and Aharonson, 2005). The average particle size across broad expanses of the south polar region has been derived from thermal inertia measurements to be consistent with silt-size particles, 50–200 μm in diameter (Paige et al., 1994; Paige and Keegan, 1994), which we will refer to as “fines” for the remainder of this paper.

Dark (relative to ice) fines form spots and fans as they settle on the surface of the seasonal ice after they are carried away from the source by local near-surface winds. Eventually patches of fines lower the overall albedo of the cryptic terrain as seen by lower resolution instruments. Piqueux and Christensen (2008) calculate from the fraction of dust coverage of the cryptic region at  $L_s = 210^\circ$  that the mass of fines,  $4 \times 10^{13}$  kg, moved in the seasonal cycle every year, is equivalent to 100 times the mass of dust in a global dust storm.

Upon completion of sublimation of the seasonal ice layer the surface returns to a uniform albedo and fans are difficult or impossible to distinguish. Kieffer (2007) provided a model of the entire process including estimates for the height of inferred plumes. Fan characteristics and the gas flow implied by their morphology are modeled in Paper II (Thomas et al., this issue). The postulate that the CO<sub>2</sub> seasonal frost anneals into translucent slab ice over the course of a martian winter has been confirmed by Mars Express

Omega observations (Langevin et al., 2007), and the process is modeled in detail in Paper III (Portyankina et al., this issue).

## 1.2. Observations in the seasonal campaign

NASA’s MRO spacecraft entered its Primary Science Phase (PSP) on 6 November 2006. The campaign to observe sublimation of the southern seasonal CO<sub>2</sub> cap began in December 2006 at  $L_s = 155^\circ$ . The spacecraft is in a roughly polar, 255 km × 320 km orbit that is Sun-synchronous. The orbit periapsis is over the south pole. The spacecraft ground-track passes over the equator at 15:05 local mean time (i.e. 3:05 pm on Mars) every 112 min.

HiRISE provides images at spatial scales down to 0.25 m/px. HiRISE is a push-broom imager with a row of 10 CCDs covered with broad-band red filters. The data from the detectors are combined on the ground to produce monochromatic images that are typically 20,000 pixels wide, providing a swath of approximately 6 km width. The length of the swath can be commanded and is the result of a trade-off between coverage and data volume. Typical lengths are 40,000–80,000 lines, thus an image 12–24 km long is common. Four additional CCDs (two above and two below) in the center of the focal plane are aligned with the center red CCDs to provide 3-color coverage with blue-green (~536 nm), red (~692 nm), and near-IR (~874 nm) filters over the central 4000 pixels of the swath. See McEwen et al., 2007 for a full description of the camera.

A total of 19 locations at high southern latitudes were selected for the investigation of seasonal sublimation processes, listed in Table 1. This paper focuses primarily on the four regions shown in Fig. 1, with detailed analysis of data from the two regions informally named “Manhattan” and “Inca City”. Our objective was to get temporal coverage throughout spring, at the expense of spatial coverage, to monitor sublimation as a function of time, given by  $L_s$ .  $L_s$  is a measure of the martian season: it is the true anomaly of Mars in its orbit around the Sun, measured from the martian vernal equinox.  $L_s = 180^\circ$  is the first day of spring in the southern hemisphere. At  $L_s = 222^\circ$  one degree of  $L_s$  is ~1.6 martian days (sols). Most of our selected sites are poleward of  $-84^\circ$ N latitude, with repeat coverage as often as every few hours or days. At sites farther from the pole such as Inca City and the Russell Crater dunes repeat coverage is less frequent.

One of the goals for HiRISE study of seasonal processes was to test the “gas jet” model described above. We attempted to detect plumes of particles elevated above the surface by acquiring stereo images separated by spacing as close as every orbit. Although no plumes were detected (discussed in Paper II), the stereo images have been processed as anaglyphs, and have provided key insight into the local terrain and its effect on the morphology of seasonally-eroded terrain.

## 1.3. Araneiform terrain at HiRISE resolution

Typical araneiform (spider-like) terrain featuring radially-organized troughs in the cryptic region is illustrated in Fig. 2, one image shown at three different levels of resolution. High resolution of the swath of fans reveals that the fans are correlated with a field of araneiform channels, shown in Fig. 2b. Thin channels widen and deepen as they converge (Fig. 2c shows a typical “spider” within this field and its anaglyph). High-resolution images of areas without fans reveal a dense channel network, not radially-organized, of similar size channels, ~1 m wide (Fig. 2d). Relief detectable very early in the season shows that seasonal CO<sub>2</sub> ice conformally coats the channels, consistent with energy balance calculations (Kieffer, 2007), i.e. channels are discernible as channels, even early in the season.

Some spiders appear draped over local topography, as shown in the Fig. 3 anaglyph. Often channels grow larger as they go

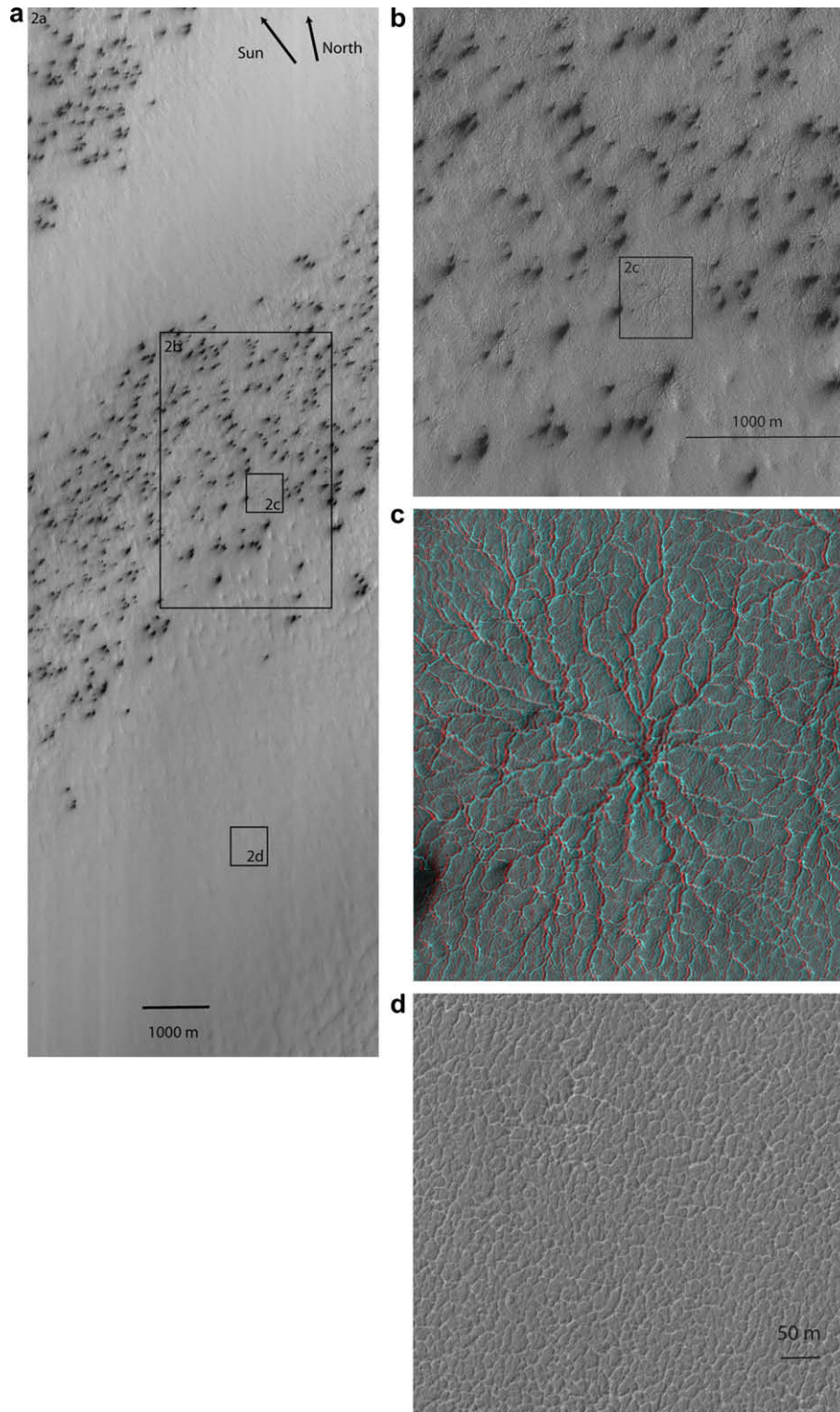


**Fig. 2.** Typical examples of araneiform (spider-like) and “lace” morphologies are illustrated. The four images shown are all from PSP\_002532\_0935, telescoping from the full HiRISE field of view (a), to full resolution in the HiRISE image (d). All sub-images have the sun coming from the upper left. (a) This HiRISE image shows a typical scene in a region of the cryptic terrain informally called Manhattan. The center latitude/longitude of this image is  $-86.399^{\circ}\text{N}$  (planetocentric)/ $99.05^{\circ}\text{E}$ . The image is  $5.4 \times 16.6$  km, and shows regions with and without fans. The  $L_s$  was  $181^{\circ}$ , early in southern spring, at a time when this region is covered with seasonal  $\text{CO}_2$  ice. The location shown for 2d is approximate. (b) Zooming in on the region of the (a) image with multiple fans, a field of “spiders” becomes discernible. (c) The relief detectable in this typical “spider” at the full HiRISE scale (0.26 m spatial scale, which corresponds approximately to 0.5 m resolution) shows that these “spiders” are channels carved into the substrate. The spider is  $\sim 500$  m diameter. The anaglyph of our case-study “spider” was produced from PSP\_002532\_0935 and PSP\_002533\_0935 acquired one orbit later. The left eye is red. (d) This sub-image is taken from the area that shows no fans. Close-up inspection at full HiRISE resolution shows that there are channels here also but they are no longer radially organized – instead they form a dense network, dubbed “lace”.

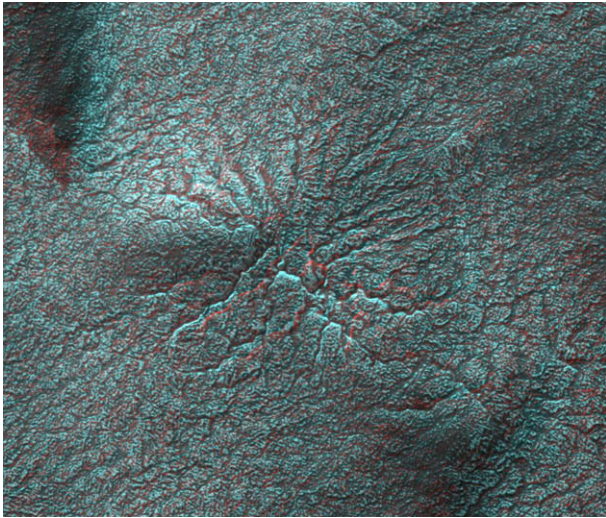


**Fig. 3.** The anaglyph of this “spider” shows channels widening uphill. This is consistent with gas rather than liquid as the erosive agent. PSP\_003363\_0945 and PSP\_003364\_0945, acquired at planetocentric latitude/longitude =  $-85.4^{\circ}\text{N}/103.9^{\circ}\text{E}$ ,  $L_s = 220^{\circ}$ , were used to create this stereo pair.

uphill – implicating pressurized fluid as the erosive agent. If we interpret the channels as carved by end-to-end fluid flow, this means that at some part of the channel the fluid flowed uphill, which can only occur for a confined flow. Thus, this observation excludes formation of spiders by any kind of sub-aerial gravity-driven flow. Erosion of the channels by flow of pressurized gas beneath a slab of  $\text{CO}_2$  ice is consistent with this observation.

At HiRISE resolution fans are seldom seen to come from the center of a spider – rather they typically come from locations along the channels. This is a new finding as older hypotheses based on lower resolution MOC images predicted that the gas flow would be towards the center, and that the fans would emanate from the center (Piqueux et al., 2003; Kieffer, 2007). Our interpretation is that gas flows to a rupture that has occurred at a weak point in the overlying ice, which may or may not occur at the center. This observation is not necessarily at odds with the model developed by Kieffer (2007), as his calculation of sub-slab gas flow velocity and scour potential is based on the regional sublimation rate and conservation of mass, not on details of the channel morphology.

## 2. Study areas

### 2.1. Manhattan

The araneiform terrain illustrated in Fig. 2 is in a region known informally as Manhattan. This region was first investigated using Odyssey’s THEMIS data (Christensen et al., 2005; Kieffer et al., 2006). A series of HiRISE images were acquired at planetocentric latitude/longitude =  $-86.387^{\circ}\text{N}/99^{\circ}\text{E}$ , as listed in Table 1 of Paper II. Fig. 13 in Paper II shows the time sequence of images acquired at this site, zooming in on the spider shown here in Fig. 2, from completely frost-covered to bare ground. The earliest images were acquired at  $L_s = 181^{\circ}$ , just a short time after the Sun rose over the horizon. Fan-shaped deposits are already evident, implying that gas jet activity and erosion of fines from the surface has already started. Portyankina’s translucent ice model (Paper III, this issue), which predicts the amount of energy that will reach the base of the  $\text{CO}_2$  cap, shows a steep increase in available energy as soon as the Sun peaks over the horizon. At a latitude of  $-85^{\circ}\text{N}$  her model predicts that the ice will crack as early as  $L_s = 176^{\circ}$ . MOC images (at this latitude but a different longitude) show sublimation spots

appearing even before sunrise (Aharonson, 2004). MRO’s afternoon orbit precludes acquisition of images early enough to detect the onset of the gas jet activity. The sites are not illuminated until later – the images of Manhattan acquired at  $L_s = 181^{\circ}$  have an incidence angle of  $88.1^{\circ}$ .

High resolution imaging after all seasonal ice is gone allows determination of the channel depths; see Fig. 4. This spider is  $\sim 500$  m in diameter. Channels are many meters wide, slowly narrowing with distance from the center. Depths of the channels carved into the surface were measured from shadow lengths. The depth in the center is  $1.8 \pm 0.3$  m. The depth of the channels decreases gradually with distance from the center, as noted in measurements made at the points illustrated. The diameter of this araneiform feature is typical in Manhattan – in a  $5 \text{ km} \times 3.5 \text{ km}$  area we counted 63 spiders, or  $\sim 4$  spiders/ $\text{km}^2$ , in contrast to Inca City, described below.

Surface material is redistributed every season in Mars’ sub-ice sublimation-driven erosional process. What appear to be deep drifts of fines from fan-shaped deposits on the underlying ice, muting the apparent relief, are shown in Fig. 5. The drifts appear to partially fill the channels. When the ice is gone the fans are no longer discernible, and channels appear somewhat mantled. Quantification of the extent to which channels can be filled in one Mars year must await images acquired over a timescale of multiple Mars years. Close inspection of the surface with its patterns of crisscrossing shallow channels raises the question of whether shallow channels were deeper in the past, and have been filled in, or whether they are simply younger. Either possibility shows reworking and redistribution of surface material and leads us to conclude that local redistribution of surface material is the most active surface-shaping process on Mars today, consistent with calculations in Piqueux and Christensen (2008).

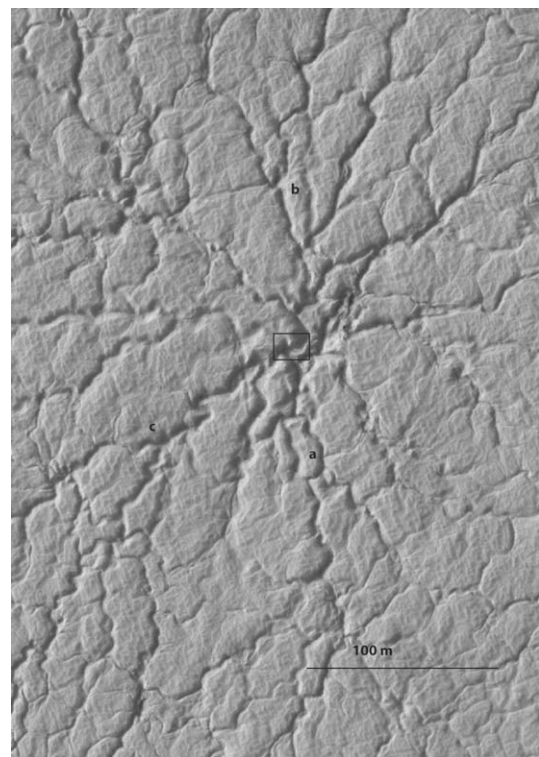


**Fig. 4.** After sublimation of seasonal frost (image acquired at  $L_s = 325^{\circ}$ ) a sub-image of the spider identified in Fig. 2 was used to measure channel depths from shadows: center depth = 1.8 m, channel a: 5 m wide, 1 m deep; channel b: 3.4 m wide, 0.7 m deep; channel c: 5 m wide, 0.6 m deep. In this image, PSP\_005579\_0935, shown at full resolution, the incidence angle =  $74.88^{\circ}$ .

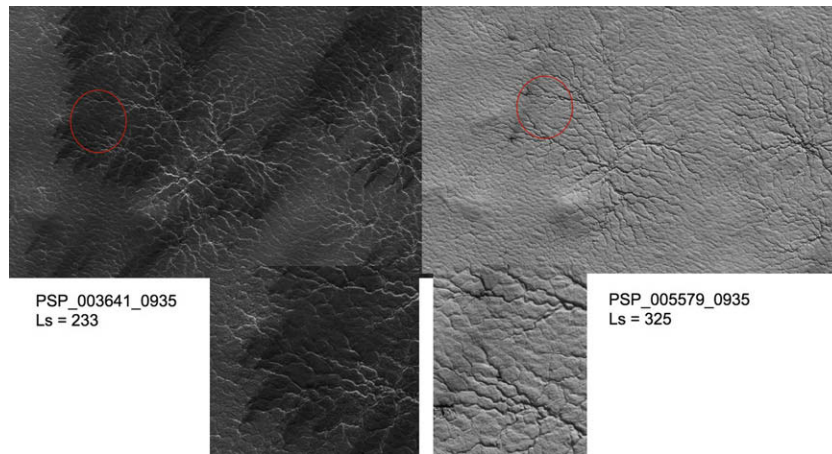


**Fig. 5.** Drifts of fines appear to lie in thick deposits that obscure underlying channels. In the locations circled below, the image on the left shows deep drifts of fines. The image on the left is PSP\_003641\_0935; the one on the right is PSP\_005579\_0935. Both are members of the time series for Manhattan shown in Fig. 2, with the image center planetocentric latitude/longitude =  $-86.39^\circ$  (planetocentric)N/ $99.08^\circ$ E. The image on the right is completely free of seasonal ice. Channel relief is muted, however we cannot quantify how much channel burial may have taken place this season. This area will be imaged again in the next martian spring to see if annual changes are detectable. The sub-images are  $\sim 1$  km wide. North is to the right.

We compare the araneiform terrain shown in Fig. 2b to the region of unorganized channels (dubbed “lace”) shown in Fig. 2d, just a few kilometers away. In this lace terrain fans appear at a much later  $L_s$  than in the araneiform terrain. In Fig. 6a, acquired on  $L_s = 226^\circ$ , there are just a few fans in the vicinity of Fig. 2d. In Fig. 6b, acquired on  $L_s = 233^\circ$ , numerous fans have shown up in the lace terrain, but the fines are mobilized in smaller fans. As seen in Fig. 6c the fans are more evenly distributed.

Comparison of these images of Manhattan to MOLA topography, illustrated in Fig. 7, shows an interesting relationship between the lace, the araneiform terrain, and the topography, even though the range of elevation is less than 300 m. The araneiform terrain is on slightly steeper slopes of 2.6%. The lace is found at higher elevation, but also is on slightly shallower slopes of 1.5%. High resolution anaglyphs suggest that small scale undulation in the terrain also plays a role, with lace occurring on planar, albeit slightly tilted, ground, and spiders sprawled over small rises. The degree of cementation of the substrate may however be the dominant factor.

## 2.2. Inca City

“Inca City”, the informal name for the second site selected for in-depth case study, is located at  $-81^\circ$ N/ $296^\circ$ E. An MRO Context Imager (CTX) image is shown for regional context relative to the outline of the HiRISE footprint in Fig. 8. It is an interesting region to study sublimation effects because of the large range of surface slopes and orientations, which allow us to study different causes and effects. The data set for Inca City is shown in Table 1 of Paper II, which indicates that data were acquired over a range of  $168^\circ$  of  $L_s$ .

Inca City has a large number of relatively steep slopes and the MOLA interpolated data set indicates that these slopes exceed  $13^\circ$  in many places (Fig. 9). On these slopes there are commonly what appear to be cracks or sharp changes in the local slope. These structures are often, but not always, the sources of gas jet activity. The structures have an almost polygonal appearance although the cracks perpendicular to the local slope seem to be most prominent. However, this latter observation might be primarily the result of the illumination. The polygonal appearance finishes abruptly at the bottom of the slopes. The ridges also show very little evidence of such a structure.

In the Inca City region, there are two distinct types of araneiform structures (Fig. 10). “Fat” spiders have a large central depression and the thin troughs that emanate radially from the center are

short and relatively wide compared to those in Manhattan. In order to quantify the qualitative observation that there is a high areal density of features, we conducted a count in an  $800\text{ m} \times 800\text{ m}$  area and found  $192 \pm 8$  features per square kilometer. (The reported uncertainty reflects the fact that it is sometimes difficult to count features that overlap.) Determination of diameter of the central depression is prone to error because of the roughness of the edges and the non-circularity of many of these spiders. For the 128 spiders in the  $800\text{ m}^2$  test area, the mean diameter is 43.6 m with a standard deviation of 9.9 m (although the distribution is, of course, not a symmetric Gaussian). Assuming an average 2 m depth at the center and oblate ellipsoidal shape, then we obtain a typical volume of  $\sim 8 \times 10^3\text{ m}^3$  (comparable to the estimate of  $10^4\text{ m}^3$  from Piqueux and Christensen (2008)).

The other type of spiders we observed in Inca City have large, rough centers with long, thin troughs extending outwards. The surface density of these features is much lower:  $36 \pm 8$  features per square kilometer. These larger spiders often seem to be related to terrain that exhibits polygonal cracks (Fig. 11). The channels connected to the centers of the spiders may simply be enlarged cracks that were originally part of the polygon network (Piqueux and Christensen, 2008). The centers of the spiders often appear to contain blocks that have been partially eroded.

The density distribution, the extensive nature of the large thin spiders, and the clear relationship to polygonal cracks indicate that the fat spiders and the larger, thinner spiders are distinct species – one cannot evolve into the other through erosion. Furthermore, as shown in Fig. 10, the different types are usually seen in separate areas within the study region and only rarely in proximity to each other.

For both types of araneiform structure, some of the sinuous channels leading away from the centers intersect. There are also channels that appear to link spiders with their neighbors. There are many examples of this in the Inca City region and some are evident in Fig. 10. In the deepest depressions within the Inca City structure, the araneiform features appear to have reached the point where they appear to be fully evolved, i.e. the spider structures are superimposed upon each other and clear separation of one from another is not possible. The channels are linked and the surface as a whole has no regular pattern. In Inca City, two adjacent local topographic minima contain two different types of spider (the fat and the long thin species) but in both cases, it appears that they have evolved in a similar way to produce superimposed, strongly-linked surface structures.

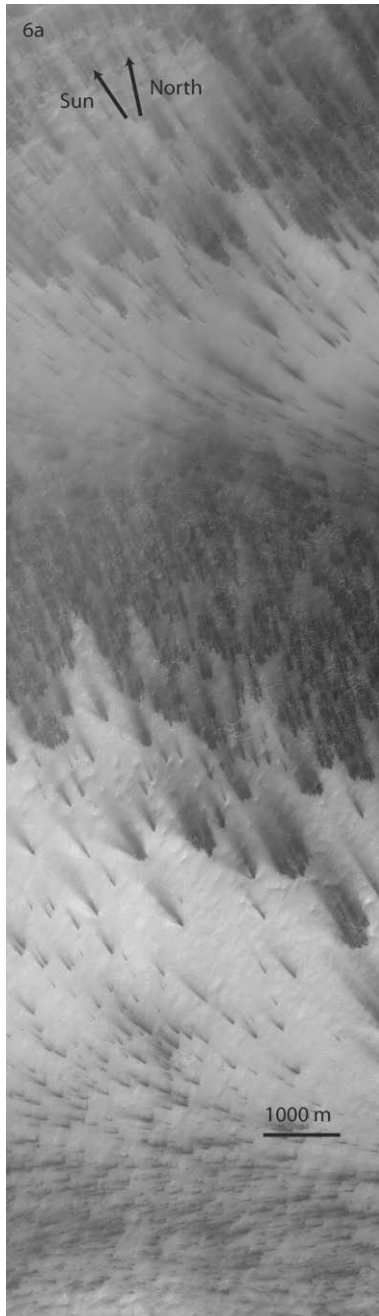


**Fig. 6a.** Image PSP\_003496\_0935 was acquired at  $L_s = 226^\circ$ , in the same location (latitude/longitude =  $-86.39^\circ\text{N}/99.0^\circ\text{E}$ ) as Fig. 2. Only a few fans have emerged in the vicinity of the lace terrain shown in Fig. 2d. The fan orientation is different than in the araneiform terrain of Fig. 2b, reflecting the change in wind direction.

In another region of Inca City, shown in Fig. 12, we see crudely aligned troughs with jagged sides. The alignment of the larger troughs may be linked to the local terrain. A network of smaller troughs extends outwards from the troughs, in some cases linking the larger troughs. In the lower right corner of Fig. 12, one can see a structure that resembles a large thin spider. If some part of the trough were to erode outwards, perpendicular to the trough direction, a structure similar to a large thin spider might result. However, large thin spiders seen elsewhere are not linked by troughs. This suggests that this could be a different style of erosional phenomenon, or the same process with different material properties.

In Inca City araneiform features and seasonal fans are found in a place where translucent ice has not previously been unambigu-

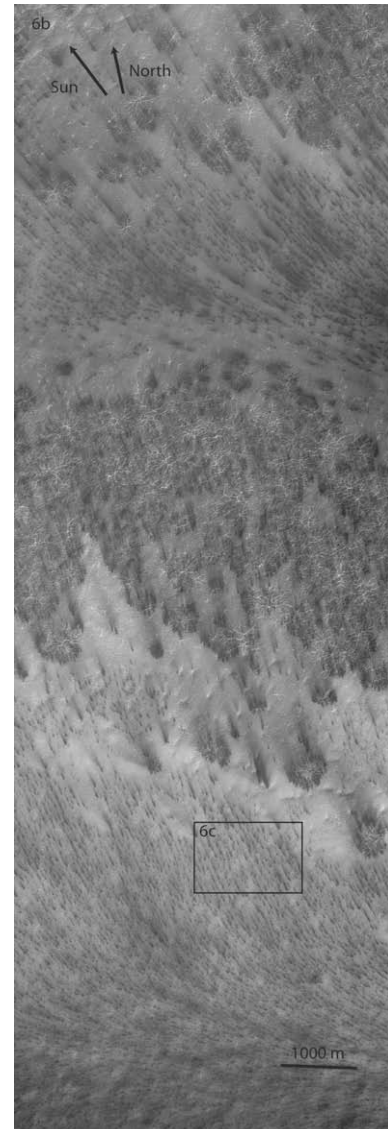


**Fig. 6b.** Fourteen sols later the lace terrain is now dotted with numerous small fans. Image PSP\_003641\_0935 was acquired at  $L_s = 233^\circ$ .

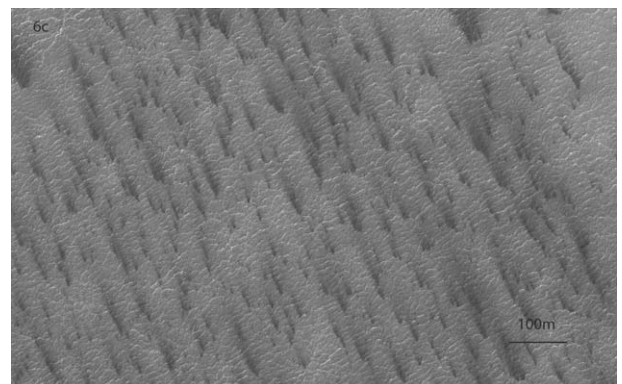


**Fig. 6c.** This sub-image of PSP\_003641\_0935 shows that the fans in the lace terrain tend to be smaller and more evenly distributed compared to the araneiform terrain.

ously identified, although dark patches seen in MOC images could be slab ice (Malin et al., 1998). The evidence for sublimation from the base of the seasonal  $\text{CO}_2$  ice layer presented by araneiform

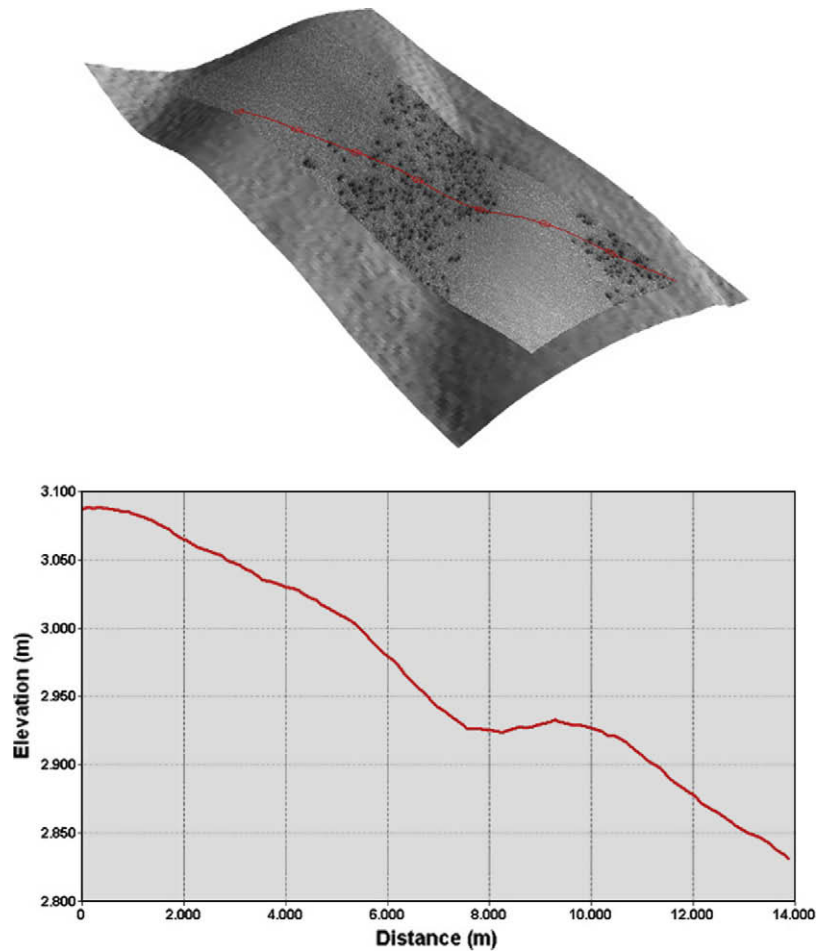


**Fig. 7.** HiRISE image PSP\_002532\_0935 (shown in Fig. 2) is shown draped over MOLA topography. The tick marks on the profile in the perspective view line up with the (south end of image) 0, 2, 4, 6, 8, 10, and 12 km (north end of image) lines in the plot. Lace terrain is in the 0–4 km portion of the image, on a slope of 1.5%. Araneiform terrain covers 4–8 km, on a slope of 2.6%.

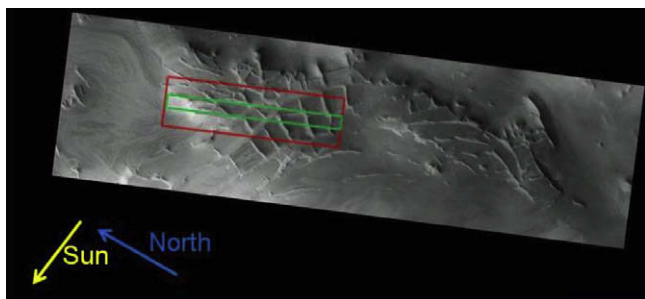


**Fig. 8.** A typical HiRISE footprint is superimposed on this CTX image of the Inca City region of the south polar region of Mars (latitude/longitude =  $-81^{\circ}\text{N}/296^{\circ}\text{E}$ ). HiRISE imaged this region in detail throughout southern spring and summer. The central green box indicates a typical region for which HiRISE three color imaging was obtained. (For interpretation of the references to color in this figure legend, the reader is referred to the web version of this article.)

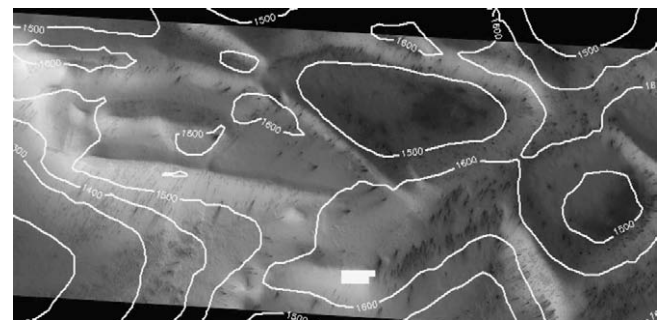


**Fig. 9.** A contour map of topography derived from the MOLA experiment has been superimposed upon a geometrically rectified version of HiRISE image PSP\_002868\_0985. The elevation ranges from below 1200 m in the lower left corner to a maximum elevation of just over 1700 m. The maximum slope within the field is  $35^{\circ}$  but one must recall that the interpolated MOLA map has a resolution of 115 m and hence steeper slopes at smaller spatial scales are possible. The contours are at 100 m intervals. The swath width (from top to bottom in this image) is 5.1 km wide.

features and fans implies that in Inca City either (a) translucent ice does exist, perhaps for such a short time that it has not previously been identified, or (b) thermal conduction of heat from the subsurface alone provides enough energy for sublimation from the base of the ice layer to take place, with associated gas flow to vents and erosion of the surface, as proposed by Aharonson (2004). Kieffer (2007) calculates that in all cases except low thermal inertia with deep ice the seasonal heat flow will cause substantial basal sublimation.

### 3. Nomenclature and classification of sublimation-driven erosional morphologies

In just the two locations described above we see a variety of araneiform features whose morphology may be influenced by local terrain and surface material properties. To begin to generalize this

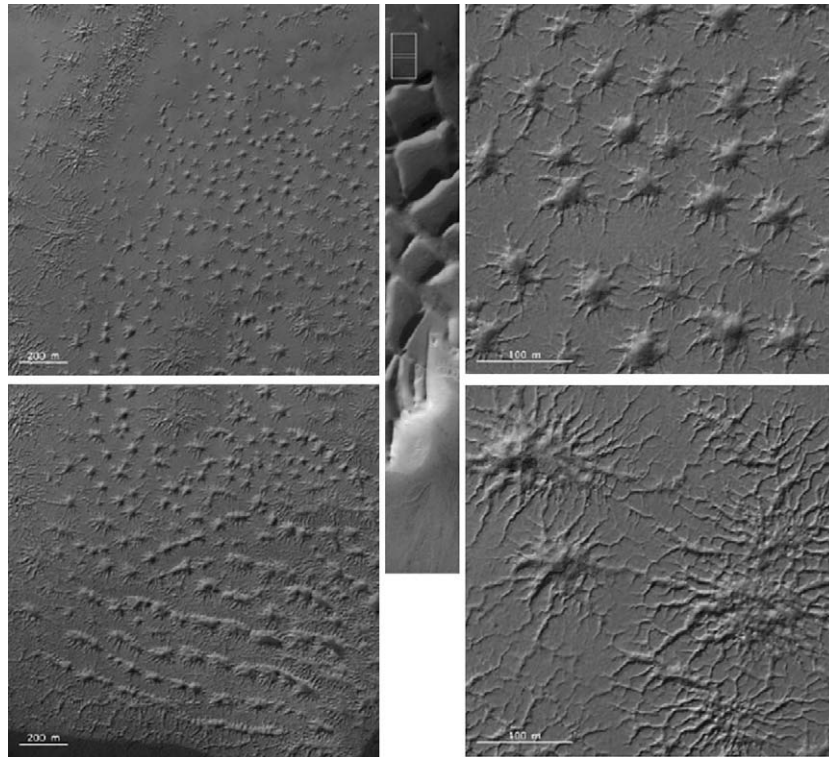


**Fig. 10.** Proximity and differences in appearance between fat spiders and the thin extended spiders. Center: Full image PSP\_005993\_0985, centered at  $-81.37^{\circ}\text{N}/295.85^{\circ}\text{E}$ , with a box indicating the approximate position of the enlarged sub-images. Top left: A higher resolution sub-frame showing that “fat” and “thin” spiders are clearly separated. Some thin spiders are seen within fat spider fields however. Top right: Fat spiders show a higher surface density with short channels emanating from the center. Bottom right: Thin spiders for comparison at the same scale. Bottom left: Fat spiders are aligned and appear to be topographically controlled. The local slope is downwards (as deduced from the MOLA map of the region) towards the top of this sub-frame, although shallow.

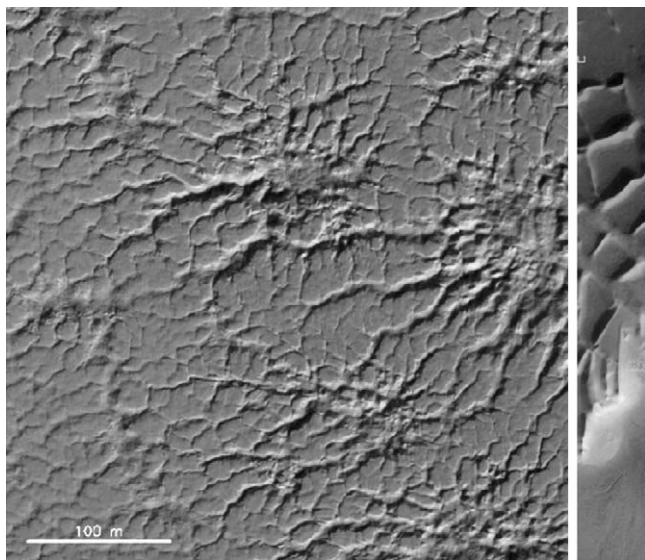


**Fig. 11.** Larger araneiform structures appear to be related to polygonal terrain. In this sub-area of image PSP\_005993\_0985 (indicated by white box in full frame on the right) we see several large spiders but the entire area shows polygonal cracks. The channels leading to the centers of the spiders may simply be enlarged cracks that were originally part of the polygon network (see also Piqueux and Christensen, 2008).

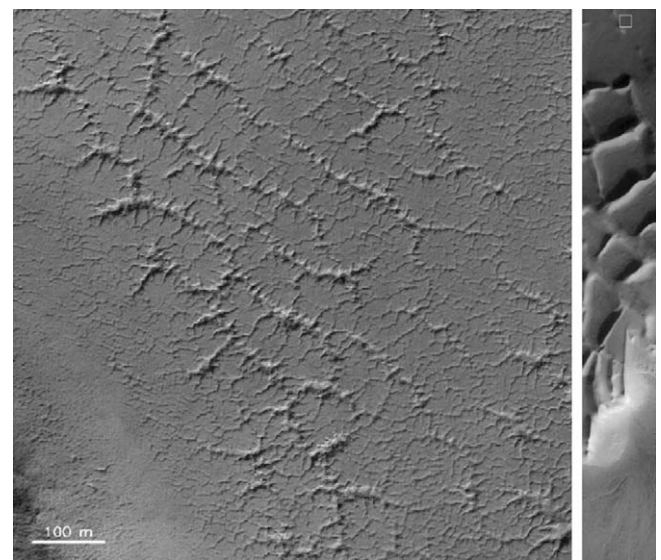


**Fig. 12.** PSP\_005993\_0985 sub-image showing jagged troughs in the surface that are roughly aligned and partially linked by dendritic structures. The white box in the panel on the right indicates the location of the sub-image in the full frame.

interpretation it is important to start classifying the morphology of the surface erosional features: a new classification scheme will allow us to begin to correlate particular kinds of structures with underlying terrain, surface material properties, and differences in

the insolation the features receive. A complete taxonomy will of course require much more extensive high resolution imaging coverage of the south polar region, however we initiate the categorization process with the available data set.

There is some overlap of sublimation-driven morphology with polygonal networks of cracks generated by contraction of ground

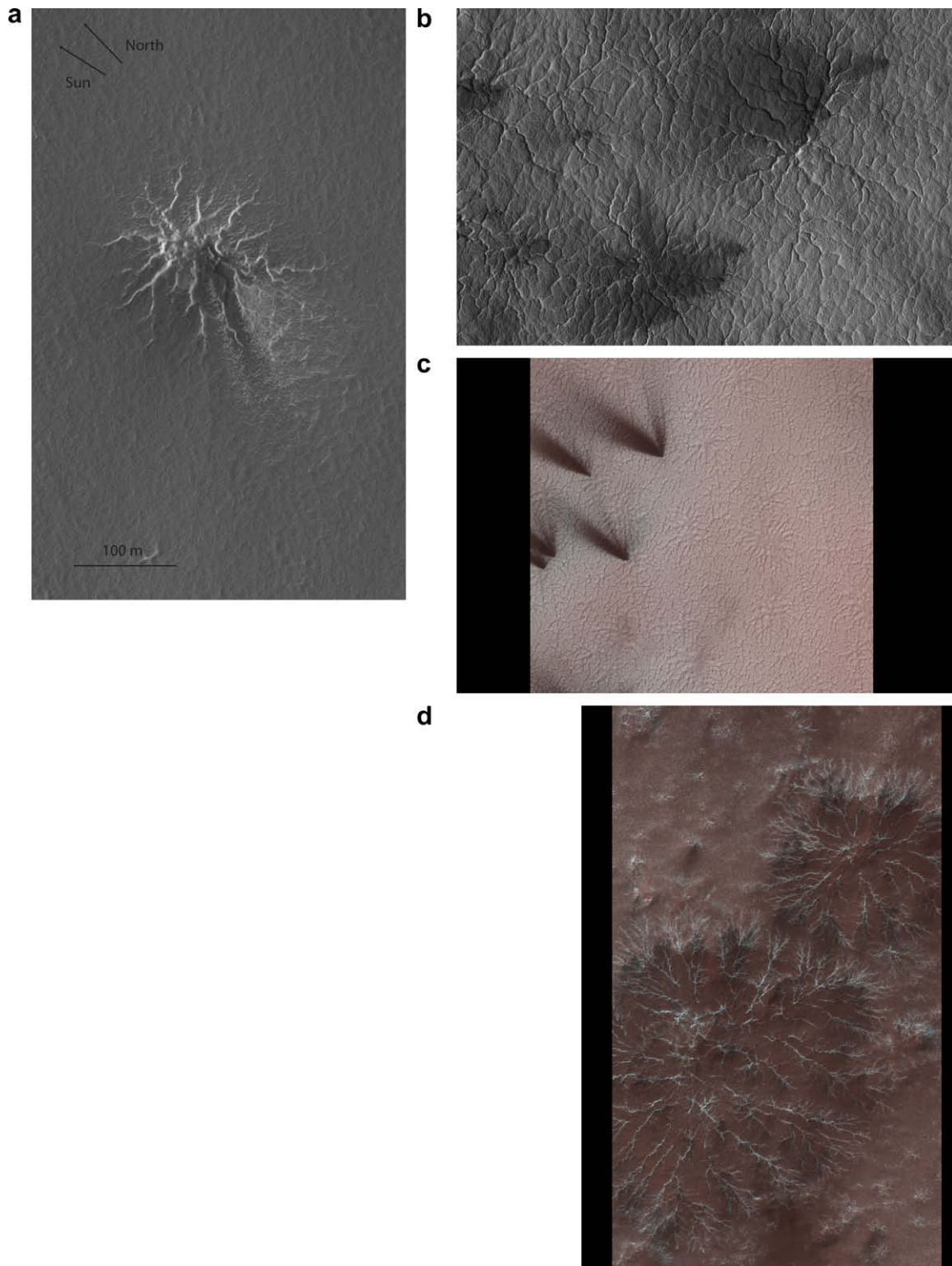


**Fig. 13.** Subcategories of araneiform morphologies, in addition to those identified for Inca City and Manhattan, are illustrated here. (a) Isolated Araneiform Morphology. This subimage of PSP\_003087\_0930 shows a “classic” spider with radially organized channels, relatively isolated, and a fan of fines emanating from near the center. The image was acquired at  $L_s = 206^\circ$ , with a center at planetocentric latitude/longitude of  $-87.12^\circ\text{N}/126.302^\circ\text{E}$ . The sub-image is 575 m wide. (b) Connected Araneiform Morphology. Image PSP\_002850\_0935 was acquired at  $L_s = 195^\circ$ , planetocentric latitude/longitude =  $-86.387^\circ\text{N}/99.0^\circ\text{E}$  (Manhattan region). This sub-image at full HiRISE resolution shows spidery, radially-organized channels branching and connecting. (c) Etched Araneiform Morphology. PSP\_003364\_0945, features broad channels on flat terrain, at planetocentric latitude/longitude =  $-85.4^\circ\text{N}/103.9^\circ\text{E}$ ,  $L_s = 220^\circ$ . The width of this sub-image is  $\sim 1$  km. This is a false-color image, used because the terrain shows up best in color. (d) Starburst Araneiform Morphology. These large “spiders” are roughly circular and do not connect. This is a sub-image of PSP\_003443\_0980, acquired on  $L_s = 223^\circ$ , centered at planetocentric latitude/longitude =  $-81.8^\circ\text{N}/76.1^\circ\text{E}$ . The sub-image is  $\sim 1$  km wide. This is a false-color image, used because the terrain shows up best in color.

ice (Mellon, 1997) that shape the surface. Subsurface cracking due to thermal stresses in ground ice may create the initial weakness in

the surface that is subsequently exploited by the escaping  $\text{CO}_2$  gas, which then erodes surface material forming the channels we see.

Classification criteria considered are:

1. Are the erosional channels radially organized? If yes this is araneiform terrain.
  - a. Do spider-like channels connect to each other or are they isolated?
  - b. How wide and deep is the central depression?
  - c. How wide and deep are the channels relative to the central depression?
2. Are the channels relatively uniform in size and depth, networked together rather than radially organized? If yes this is lace terrain.
  - a. What is the degree of tortuosity of the channels?
3. Are the channels not channels at all, but rather grooves in patterned ground serving as conduits for gas and fines? In this case the channels are shallow and exhibit the regularity of form identified in Mangold (2005).

“Araneiform” morphology features radially-organized channels, which widen and deepen towards the center. This type of terrain is associated with numerous fans, which show up very early in the season. Examples have been shown in Fig. 2b (connected spiders in Manhattan) and Fig. 10 (fat spiders and thin spiders in Inca City). More examples of araneiform categories of morphology are shown in Fig. 13a–d, which come from other locations in the south polar region. An individual “spider” may range in size from tens of meters to 1 km in diameter. They may be isolated or their channels may connect as in Figs. 13a and 13b, respectively. Terrain in Fig. 13c features broad shallow radially-organized channels. Fig. 13d may be an example of extreme amounts of fines choking off gas flow in the center of the spider, resulting in growth and branching of channels further from the center.

“Lace” refers to dense networks of channels that are similar in size. Sub-categories of lace morphologies are distinguished by the degree of tortuosity of the channels, ranging from short straight segments to extremely kinked segments. Examples of lace terrain are shown in Figs. 2d, 6c, 14a and 14b. Channels are not radially organized. Fewer fans are observed in these regions, and the fans emerge later in the season, which may imply that the gas release here is a more diffuse steady-state process that builds up less pressure, limiting its capacity to entrain loose fines. Networks of channels with short straight segments may be eroded patterned ground without a clear cutoff between the two categories. Highly tortuous networks with kinked segments are not consistent with linear cracking of ground ice and are more reminiscent of the sinuous morphologies associated with low energy fluid flow.

Patterned ground with shallow grooves is shown in Fig. 15a (covered with seasonal ice) and Fig. 15b (bare ground). This type of terrain is common in the region known informally as Ithaca. Numerous fans emerge early in the season. Fig. 15c shows rectangular patterned ground in the region known informally as Giza. Patterned ground at high latitudes on Mars has been mapped and divided into classes by Mangold (2005) based on MOC images, attributed to substrate thermal stresses, but the erosional agent provided by sub-ice sublimation of CO<sub>2</sub> was not considered in detail. The relationship between polygonal networks and CO<sub>2</sub> sublimation has been analyzed by Piqueux and Christensen (2008).

There are intermediate cases between araneiform and lace in which some channels are deeper than others, but are not organized radially. More than one type of morphology is often observed within a single image. A transitional region from lace to araneiform terrain is shown in Fig. 14b.

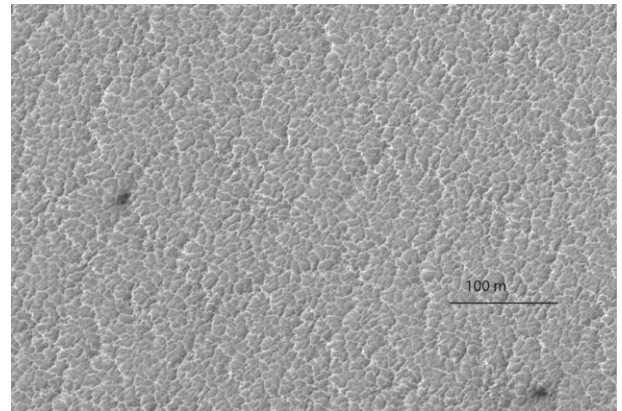


**Fig. 14a.** Lace morphology is characterized by numerous connected channels that have varying degrees of tortuosity. This sub-image from PSP\_002652\_0930 shows a network of channels, like lace, not radially organized. This image was acquired at planetocentric latitude/longitude =  $-87.0^{\circ}\text{N}/98.13^{\circ}\text{E}$  (Manhattan),  $L_s = 186^{\circ}$ . Comparison of this image with Fig. 2d shows the variability of tortuosity in lace terrain. North is up, and the sun is to the upper left.

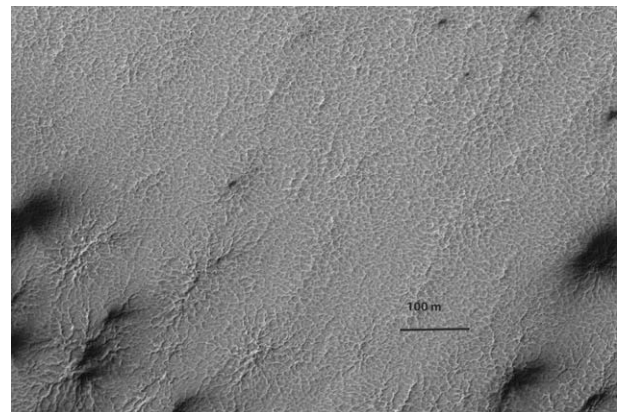


**Fig. 14b.** This sub-image from PSP\_002652\_0930 shows the transition from lace terrain at the top to connected spiders.

#### 4. Possible topographic control of structure evolution

In Fig. 10, Inca City, we can see an excellent example of how spiders can be aligned in rows indicating that the position of their initiation is not a completely random process. The lines of spiders seen here are approximately orthogonal to the direction of the local surface slope. This may be the consequence of having a line of local weakness in the substrate resulting from the slope or the production of the slope. If this leads to a weakness in the CO<sub>2</sub> slab directly above it there may be preferential outgassing along that line. Alternatively, the slope may not be constant. A small change in slope along a line may have produced a local line of weakness in the overlying CO<sub>2</sub> slab (e.g. some type of slumping) leading again to a preferred line for gas jet activity. The jagged trough structure in Fig. 12 may be related to this type of aligned spider structure although this is somewhat speculative.

The steepest slopes in the Inca City region show no evidence of araneiform structures. From these observations alone, one could conclude that spider initiation and evolution requires a low surface slope. We have identified one place on a slope that has an araneiform-like structure but it is poorly ordered – it does not show a clear center with channels propagating outwards in the “classical” sense. If the slope is steep, as is frequently the case in the Inca City region, then slumping or collapse of channel walls may occur almost as soon as they initiate, preventing spider formation.

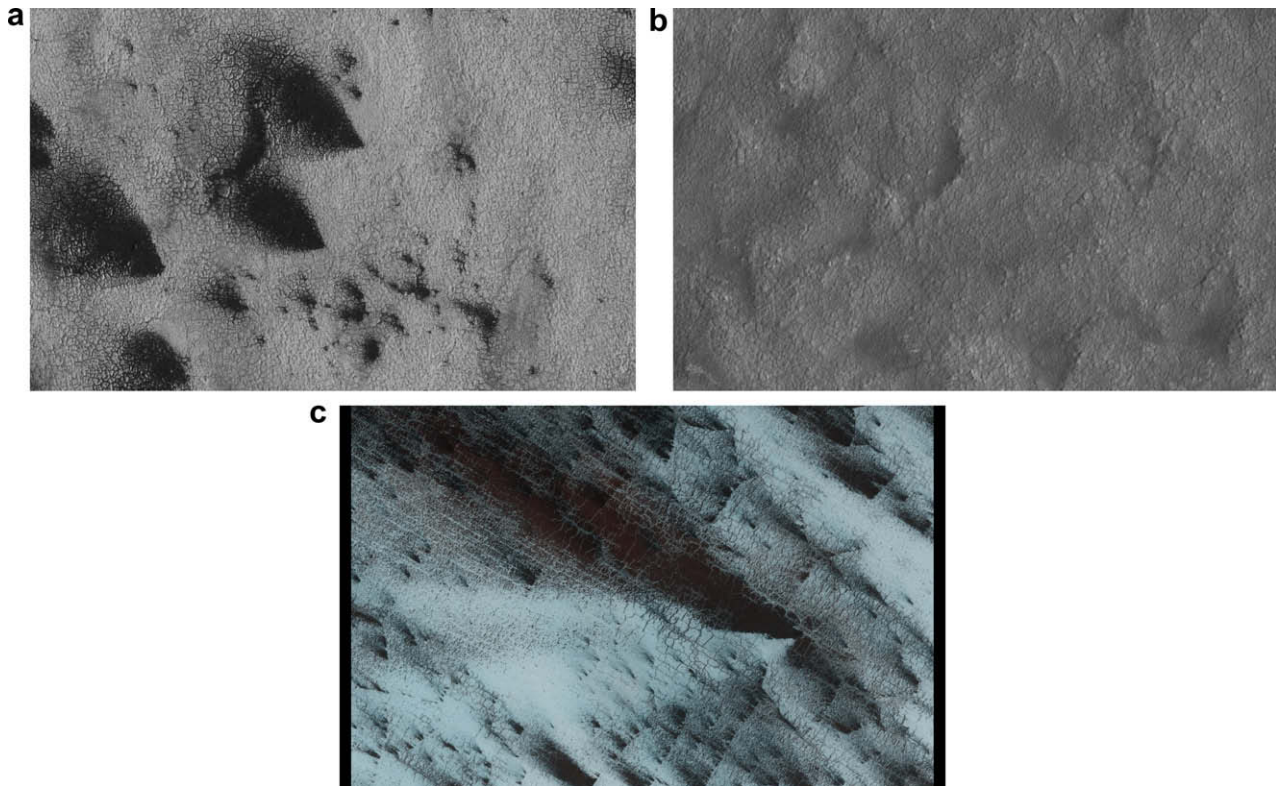


**Fig. 15.** Patterned ground formed by thermal stress and subsequent cracking of the underlying water ice-cemented ground has shallow grooves that are likely to be used as pathways for gas from the subliming CO<sub>2</sub> seasonal cap. Fans appear early in the season. (a) Patterned ground with fans is shown in this sub-image (~750 m wide) of PSP\_003730\_0945 acquired in a region informally known as Ithaca, planetocentric latitude/longitude =  $-85.2^{\circ}\text{N}/181.4^{\circ}\text{E}$ . This terrain was covered with seasonal ice at the time the image was acquired on  $L_s = 237^{\circ}$ . (b) The same terrain as in (a) is shown in this sub-image of PSP\_004891\_0945, now defrosted at  $L_s = 294^{\circ}$ . (c) Rectangular patterned ground is illustrated in this sub-image of PSP\_003474\_0850, acquired in a region known informally as Giza, centered at planetocentric latitude/longitude =  $-84.8^{\circ}\text{N}/65.7^{\circ}\text{E}$ . Sources of fans align with the grooves of the patterned ground. This sub-image is  $\sim 1$  km across. This is a false-color image, used because the terrain shows up best in color.

As shown in Fig. 16, araneiform terrain will form along the sides of ridges when the slopes are not steep. Structural control is again implicated by the alignment of the spiders with the ridges. In Manhattan and Giza, spiders form preferentially in gently undulating terrain (and in the example shown in Fig. 7 on a slope of 2.6%). Anaglyphs show that lace channels are found on ground with very little local undulation of the surface although there may be a gentle overall slope. As shown in Fig. 17, channels are eroding the edges of uppermost layers, and this may be a mechanism, combined with wind erosion, for removing entire layers over regions.

At this point our survey and classification is not complete enough to do more than note these trends. The ultimate morphology of sublimation-eroded surface features is likely due to a complex combination of structural control, degree of cementation of surface material, slopes, and energy available to drive sublimation and pressurize sub-ice gas flow.

## 5. Summary and conclusions

South polar terrain exhibits a wide variety of surface morphologies, dominated by the effects of CO<sub>2</sub> sublimation-driven seasonal erosion. At HiRISE resolution we see radially organized thin sinuous channels, broad shallow channels, “fat” and “thin” central depressions, connected and isolated spiders, starburst patterns which branch outward in a circle; networks of uniform channels termed “lace” with varying degrees of sinuosity; and araneiform terrain following topographic features. We suggest a classification of erosional features based on channel organization (radial or not), relationship and scale of channels to a central depression (in the case of radially-organized channels), and tortuosity of channels in the case of channel networks. The local topography (steep

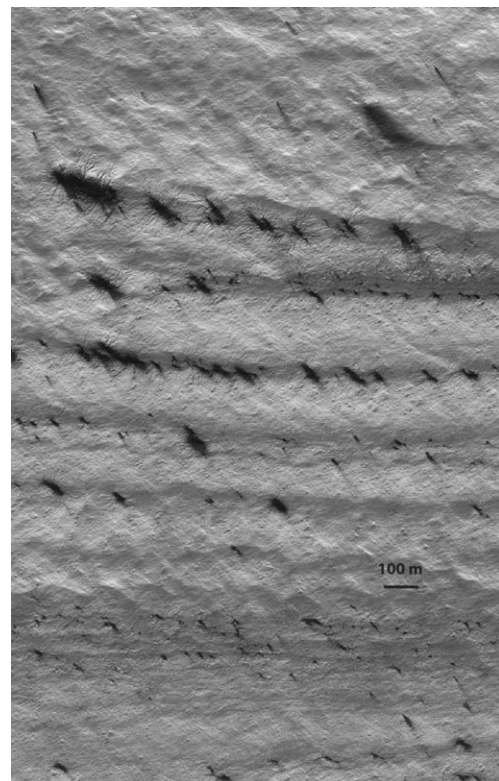


**Fig. 16.** Araneiform terrain aligned with ridges is imaged in PSP\_003140\_0935, acquired at planetocentric latitude/longitude  $-86.2^{\circ}\text{N}/94.3^{\circ}\text{E}$ , at  $L_s = 209^{\circ}$ . North is up and the sun is coming from the upper left.

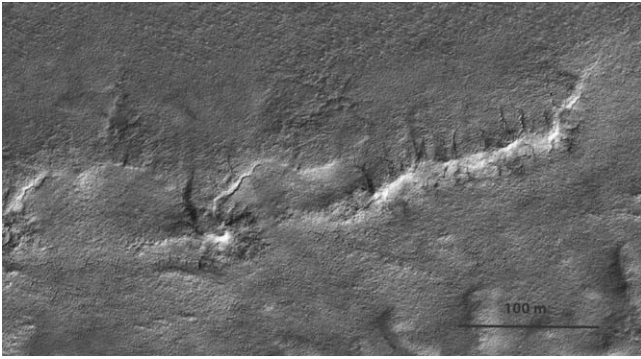


**Fig. 17.** In some images the channels are eroding the edges of uppermost layers, and may be a mechanism, combined with wind erosion, for removing entire layers over regions. This appears to be the case in PSP\_006207\_0940, acquired at planetocentric latitude/longitude =  $-85.9^{\circ}\text{N}/235.7^{\circ}\text{E}$ ,  $L_s = 352^{\circ}$ .

slopes, undulating hills, flat ground, patterned ground) appears to influence the manifestation of sub-ice sublimation-driven erosion as araneiform structures (fat spiders, thin spiders, etched spiders, etc.), lace, or accentuated patterned ground. Degree of cementation of the surface material probably also plays an important role. HiRISE images show that fans come from ruptures along channels, not just the center of spiders as previously thought. Araneiform terrain is found in Inca City, which implies that sub-ice sublimation and erosion can be driven by energy from subsurface thermal conduction, or that translucent ice does occur, perhaps briefly enough to have escaped detection by orbiter spectrometers.

HiRISE images show that the jet ejecta deposits blend back into the substrate surface after  $\text{CO}_2$  sublimation has completed (Paper II; Kieffer et al., 2006), setting the stage for repetition of the cycle with relatively loose material as a source for local surface material redistribution in the following year. HiRISE images also show how accumulations of fines may fill the channels, potentially choking off gas flow. Crisscrossing of shallow channels infers reworking and redistribution of surface material and leads us to conclude that local redistribution of surface material is the most active surface-shaping process on Mars, consistent with calculations by Piqueux and Christensen (2008). Constant reworking of the surface might produce loose silt-size material, as indicated by the thermal inertia derived by Paige and Keegan (1994) and consistent with Kieffer's (2007) model for saltation and entrainment of surface fines in gas jets. HiRISE images acquired in the future will investigate yearly changes and allow us to quantify the annual erosion and redistribution of surface material.

## Acknowledgments

This work was partially supported by the Jet Propulsion Laboratory, California Institute of Technology, under a contract with the National Aeronautics and Space Administration. Helpful comments and discussion came from Chris Okubo, Nathan Bridges, Laszlo Keszthelyi, Moses Milazzo, and James Wray and two anonymous reviewers.

## References

Aharonson, O., 2004. Sublimation at the base of a seasonal  $\text{CO}_2$  slab on Mars. *LPSC XXXV* (abstract 1918).  
 Aharonson, O., Zuber, M.T., Smith, D.E., Neumann, G.A., Feldman, W.C., Prettyman, T.H., 2004. Depth, distribution and density of  $\text{CO}_2$  deposition on Mars. *J. Geophys. Res.* 109, E05004. doi:10.1029/2003JE002223.  
 Boynton, W.V., and 13 colleagues, 2003. Constraints on the distribution of hydrogen in the polar regions of Mars and implications for ice formation processes. *AGU* (abstract P32-B05).

Christensen, P.R., Kieffer, H.H., Titus, T.N., 2005. Infrared and visible observations of south polar spots and fans. *EOS Trans. AGU* 86 (52) (P23c-04).  
 Hansen, G.B., 1997. The infrared absorption spectrum of carbon dioxide ice from 1.8 to 333 micrometers. *J. Geophys. Res.* 102, 21569–21587.  
 Hansen, G.B., 2005. Ultraviolet to near-infrared absorption spectrum of carbon dioxide ice from 0.174 to 1.8  $\mu\text{m}$ . *J. Geophys. Res. Planets* 110 (E9), 11003+. doi:10.1029/2005JE002531.  
 Hess, S.L., Henry, R.M., Tilman, J.E., 1979. The seasonal variation of atmospheric pressure on Mars as affected by the south polar cap. *J. Geophys. Res.* 84, 2923–2927.  
 Kelly, N.J., Boynton, W.V., Kerry, K., Hamara, D., Janes, D., Reedy, R.C., Kim, K.J., Haberle, R.M., 2006. Seasonal polar carbon dioxide frost on Mars:  $\text{CO}_2$  mass and columnar thickness distribution. *J. Geophys. Res.* 111, E03S07. doi:10.1029/2006JE002678.  
 Kieffer, H.H., 2000. Annual punctuated  $\text{CO}_2$  slab-ice and jets on Mars. *LPI Contribution #1057*.  
 Kieffer, H., 2007. Cold jets in the martian polar caps. *J. Geophys. Res.* 112, (E08005), 1–9.  
 Kieffer, H.H., Titus, T.N., 2001. TES mapping of Mars' north seasonal cap. *Icarus* 154, 162–180.  
 Kieffer, H.H., Christensen, P.R., Titus, T.N., 2006.  $\text{CO}_2$  jets formed by sublimation beneath translucent slab ice in Mars' seasonal south polar ice cap. *Nature* 442, 793–796.  
 Kirk, R.L., Soderblom, L.A., Brown, R.H., 1990. Subsurface energy storage and transport for solar-powered geysers on Triton. *Science* 250, 424–429.  
 Langevin, Y., Bibring, J.-P., Murchie, S., Vincendon, M., Poulet, F., Doute, S., Gondet, B., Kieffer, H., 2007. Evolution of the seasonal caps of Mars observed by OMEGA on Mars Express. In: *Seventh International Conference on Mars*, p. 3246 (LPI 1353).  
 Leighton, R.B., Murray, B.C., 1966. Behavior of carbon dioxide and other volatiles on Mars. *Science* 153, 136–144.  
 Litvak, M.L., Mitrofanov, I.G., Kozyrev, A.S., Sanin, A.B., Tretyakov, V.I., Boynton, W.V., Kelly, N.J., Hamara, D., Saunders, R.S., 2007. Long-term observations of southern winters on Mars: Estimations of column thickness, mass, and volume density of the seasonal  $\text{CO}_2$  deposit from HEND/Odyssey data. *J. Geophys. Res.* 112, (E03S13), 1–10.  
 Malin, M.C., Edgett, K.S., 2001. Mars Global Surveyor Mars orbiter camera: Interplanetary cruise through primary mission. *J. Geophys. Res.* 106, 23429–23570.  
 Malin, M.C., and 15 colleagues, 1998. Early views of the martian surface from the Mars Orbiter Camera of Mars Global Surveyor. *Science* 279, 1681–1685.  
 Mangold, N., 2005. High latitude patterned grounds on Mars: Classification, distribution and climatic control. *Icarus* 174, 336–359.  
 McEwen, A., and 13 colleagues, 2007. MRO's High Resolution Imaging Science Experiment (HiRISE). *J. Geophys. Res.* 112. doi:10.1029/2005JE002605.  
 Mellon, M.T., 1997. Small-scale polygonal features on Mars: Seasonal thermal contraction cracks in permafrost. *J. Geophys. Res.* 102 (E11), 25617–25628.  
 Mellon, M., Phillips, R., 2001. Recent gullies on Mars and the source of liquid water. *J. Geophys. Res.* 106, 23165–23180.  
 Mellon, M.T., Feldman, W.C., Prettyman, T.H., 2004. The presence and stability of ground ice in the southern hemisphere of Mars. *Icarus* 169, 324–340.  
 Paige, D.A., Keegan, K.D., 1994. Thermal and albedo mapping of the polar regions of Mars using Viking thermal mapper observations, 2, south polar region. *J. Geophys. Res.* 99, 25993–26014.  
 Paige, D.A., Bachman, J.E., Keegan, K.D., 1994. Thermal and albedo mapping of the polar regions of Mars using Viking thermal mapper observations, 1, North polar region. *J. Geophys. Res.* 99, 25959–25992.  
 Piqueux, S., Christensen, P.R., 2008. North and south sub-ice gas flow and venting of the seasonal caps of Mars: A major geomorphological agent. *J. Geophys. Res.* 113, E06005. doi:10.1029/2007JE003009.  
 Piqueux, S., Byrne, S., Richardson, M., 2003. The sublimation of Mars' southern seasonal  $\text{CO}_2$  ice cap and the formation of spiders. *J. Geophys. Res.* 108 (E8), 1–9.  
 Portyankina, G., Markiewicz, W.J., Hansen, C.J., Thomas, N., 2009. HiRISE observations of gas sublimation-driven activity in Mars' southern polar regions: III. Models of processes involving translucent ice 205, 311–320.  
 Prettyman, T.H., and 12 colleagues, 2004. Composition and structure of the martian surface at high southern latitudes from neutron spectroscopy. *J. Geophys. Res.* 109, (E05001), 1–9.  
 Schorghofer, N., Aharonson, O., 2005. Stability and exchange of subsurface ice on Mars. *J. Geophys. Res.* 110, (E05003), 1–16.  
 Smith, B., and 60 colleagues, 1989. Voyager 2 at Neptune: Imaging science results. *Science* 246, 1422–1449.  
 Smith, D.E., Zuber, M.T., Neumann, G.A., 2001. Seasonal variations of snow depth on Mars. *Science* 294, 2141–2146.  
 Soderblom, L.A., Kieffer, S.W., Becker, T.L., Brown, R.H., Cook II, A.F., Hansen, C.J., Johnson, T.V., Kirk, R.L., Shoemaker, E.M., 1990. Triton's geyser-like plumes – Discovery and basic characterization. *Science* 250, 410–415.  
 Thomas, N., Hansen, C.J., McEwen, A.S., Portyankina, G., 2009. HiRISE observations of gas sublimation-driven activity in Mars' southern polar regions: II. Surficial deposits and their origins. *Icarus*, this issue.  
 Titus, T.N., Kieffer, H.H., Christensen, P.R., 2003. Exposed water ice discovered near the south pole of Mars. *Science* 299, 1048–1051.